C. R. Physique 17 (2016) 555–564

Contents lists available at ScienceDirect

Comptes Rendus Physique

www.sciencedirect.com

Phononic crystals / Cristaux phononiques

Phoxonic crystals and cavity optomechanics

Cristaux phoxoniques et optomécaniques dans les cavités

Bahram Djafari-Rouhani *, Said El-Jallal, Yan Pennec

Institut d'électronique, de microélectronique et de nanotechnologie (IEMN), UMR CNRS 8520, UFR de physique, Université de Lille-1, Cité scientifique, 59652 Villeneuve-d'Ascq cedex, France

ARTICLE INFO

Article history:
Available online 12 February 2016

Keywords:
Phononic crystals
Phoxonics
Optomechanics
Theory
Photoelasticity
Moving interface effect

Mots-clés :
Cristaux phononiques
Phoxonique
Optomécanique
Théorie
Photoélasticité
Effet d'interface en mouvement

ABSTRACT

Phoxonic crystals are dual phononic/photonic crystals exhibiting simultaneously band gaps for both types of excitations. Therefore, they have the ability to confine phonons and photons in the same cavity and in turn allow the enhancement of their interaction. In this paper, we review some of our theoretical works on cavity optomechanical interactions in different types of phoxonic crystals, including two-dimensional, slab, and nanobeam structures. Two mechanisms are behind the phonon–photon interaction, namely the photoelastic and the moving interface effects. Coupling rates of a few MHz are obtained with high-frequency phonons of a few GHz. Finally, we give some preliminary results about the optomechanical interaction when a metallic nanoparticle is introduced into the cavity, giving rise to coupled photon–plasmon modes or, in the case of very small particles, to an enhancement of the electric field at the position of the particle.

RÉSUMÉ

Les cristaux phoxoniques sont des structures qui jouent simultanément le rôle de cristaux phononiques et photoniques en présentant des bandes interdites à la fois pour les deux types d'ondes. Par conséquent, en présence d'une cavité, ils sont susceptibles de confiner à la fois les phonons et les photons et de permettre une exaltation de leur interaction. Nous présentons dans cet article une revue de certains de nos travaux théoriques sur les interactions optomécaniques dans les cavités, en considérant plusieurs types de cristaux phoxoniques (bidimensionnels, sous forme de plaque ou de poutre). L'interaction phonon–photon est basée sur les deux mécanismes photoélastique et de déformation des interfaces. Des coefficients de couplage de quelques MHz ont été obtenus avec des modes acoustiques de quelques GHz. Dans la dernière partie de cette contribution, nous présentons quelques résultats préliminaires sur l'interaction optomécanique lorsqu'une nanoparticule métallique

* Corresponding author.
E-mail address: bahram.djafari-rouhani@univ-lille1.fr (B. Djafari-Rouhani).

http://dx.doi.org/10.1016/j.crhy.2016.02.001

est introduite à l'intérieur de la cavité photonique, donnant lieu à des modes plasmon–photon couplés ou à une valeur élevée du champ électrique sur la nanoparticule.

1. Introduction

Phononic crystals are periodic composite structures where the elastic and acoustic properties display a periodic variation in space (for recent reviews, see [1–3]). They can exhibit absolute band gaps in which the propagation of elastic waves is prohibited in any direction of the space and for any incidence angle. More generally, tailoring their band structure allows the control and manipulation of elastic waves and paves the way to several functionalities, ranging from sound isolation to filtering and signal processing [1,2], negative refraction and high-resolution imaging, nanoscale thermal transport managing [3], quantum information processing [4,5]. The concept of phononic crystals [6,7] followed by a few years the similar concept of photonic crystals [8,9] for the propagation of electromagnetic waves.

Phoxonic crystals are periodic structures that exhibit simultaneously band gaps for the propagation of acoustic and electromagnetic waves. Therefore, when creating defects such as a cavity or a waveguide, they have the ability to support localized modes for both photons and phonons. This high confinement of the two excitations in a small region of space would allow a significant enhancement of their interaction for the purpose of novel and high-performance optomechanical (OM) devices and applications. This topic has been intensively investigated in one-dimensional (1D) multilayer structures (see recent works in [10–12]) before having been extended to 2D and more recently to slab and strip structures.

The existence of simultaneous band gaps for phonons and photons in two-dimensional (2D) crystal structures was first demonstrated by Maldovan and Thomas [13] in square and hexagonal lattices. An absolute phononic gap can be found, whereas, in general, the photonic band gaps appear separately for transverse electric (TE) and transverse magnetic (TM) polarizations of the light. Bria et al. [14] demonstrated the possibility of an absolute band gap by using the anisotropy of the dielectric matrix in sapphire in the microwave regime. Sadat-Saleh et al. [15] studied the effect of the pattern added in the unit cell on the behavior of the band gaps.

Shortly after, similar investigations were extended to crystal slabs and in particular the most suitable geometrical parameters were defined for the realization of phoxonic crystal slabs made of a periodic array of holes in silicon [16,17]. More especially, we showed [16] the existence of dual phononic/photonic band gaps in honeycomb (and more generally boron nitride) as well as square lattices. It should be noticed that only a limited range of parameters allow the existence of absolute band gaps for both excitation, whereas more generally it is possible to obtain an absolute phononic gap together with a photonic gap of a given symmetry (odd or even with respect to the middle plane of the slab). Similar calculations were also performed for a crystal slab constituted by an array of Si pillars on a SiO_2 plate [18], allowing more possibilities for the opening of absolute photonic and phononic band gaps. Also, 1D phoxonic crystals constituted by nanobeams (or strips) were studied. In particular, we proposed a new structure consisting of a corrugated nanobeam containing an array of holes in the middle and an array of stubs on the sides [19–21]. Indeed, it was shown that the holes and the stubs are respectively favorable to create the photonic and phononic band gaps.

As mentioned above, since the phoxonic crystals have the ability of exhibiting band gaps for both phonons and photons, it becomes possible to design cavities that allow the simultaneous confinement of both acoustic and electromagnetic waves. Therefore, several theoretical and experimental works were devoted during the last five years to the study of the cavity optomechanic (OM) interaction, although in some papers the acoustic wave was not confined in the cavity. In particular, let us mention the acousto-optic interaction in different cavities inside 2D crystals [22,23], at the surface of a 2D crystal [24], in crystal slabs [25–29] including phoxonic–plasmonic slabs [30], in nanobeams [31–33,20,21], as well as in different waveguides (nanobeams and photonic fiber [34–37] and 2D crystal waveguides [38]). A review of the modeling of sound–light interaction in nanoscale cavities and waveguides was published recently [39]. Nowadays, the phoxonic crystals, also called optomechanic crystals, can be considered as a particular branch of the more general field of cavity OM [4,5,40,41] which have given rise to many striking phenomena such as laser side-band cooling and optomechanically induced transparency, and led to the realization of many micro and nanoscale OM devices for the measurement of a small amount of mass or charge or of a very short distance.

In this paper, we present a few selected examples of our recent theoretical works on cavity OM interaction in different phoxonic crystals. Section 2 will be devoted to the presentation of the mechanisms of acousto-optic interaction and the methods of evaluating the phonon–photon coupling rate. Section 3 contains some illustrations of the OM coupling in 2D [22,23], slab [28] and nanobeam [20,21] crystal structures. In Section 4, we give some new results about the effect of a gold nanowire in a 2D photonic cavity and in particular the phonon interaction with coupled photon–plasmon modes. Some conclusions are drawn in Section 5.

2. Mechanisms of optomechanic interaction and methods of calculations

The phonon–photon interaction is based on two mechanisms, namely the photoelastic (PE) and the moving interface (MI) effects. Both are due to a local variation of the dielectric permittivity induced by the presence of the acoustic strain. The former happens in the bulk of each material and is mediated by the photoelastic parameters (Pockels effect [42]), whereas the latter occurs at the boundaries of two materials and results from the motion of the interfaces during the acoustic vibrations [43,11]. A first method to evaluate the strength of the OM coupling is to use a first-order perturbation theory [44] in which the coupling rate expresses the shift of the photonic frequency mode of the cavity induced by the zero-point motion of the mechanical field. Its expression can be obtained from the knowledge of the acoustic and optic fields inside the cavity and is given by [33]:

$$g_{\mathrm{PE}} = -\frac{\omega}{2}\frac{\langle E|\delta\varepsilon|E\rangle}{\int_V \mathbf{E}\cdot\mathbf{D}\,\mathrm{d}V}\sqrt{\hbar/2M_{\mathrm{eff}}\Omega} \tag{1}$$

$$g_{\mathrm{MI}} = -\frac{\omega}{2}\frac{\oint_{\partial V}(\mathbf{U}\cdot\mathbf{n})(\Delta\varepsilon\mathbf{E}_{\parallel}^2 - \Delta\varepsilon^{-1}\mathbf{D}_{\perp}^2)\,\mathrm{d}S}{\int_V \mathbf{E}\cdot\mathbf{D}\,\mathrm{d}V}\sqrt{\hbar/2M_{\mathrm{eff}}\Omega} \tag{2}$$

Here $\mathbf{U}$ is the normalized displacement filed ($\max\|\mathbf{U}\| = 1$), $\mathbf{n}$ is the outside normal to the boundary, $\mathbf{E}$ is the electric field, and $\mathbf{D}$ is the electric displacement field. ε_1 and ε_2 are the dielectric permittivities of the materials on both sides of an interface, $\Delta\varepsilon = \varepsilon_1 - \varepsilon_2$ and $\Delta\varepsilon^{-1} = \varepsilon_1^{-1} - \varepsilon_2^{-1}$. $\delta\varepsilon_{ij} = -\varepsilon_0 n^4 p_{ijkl} S_{kl}$, where p_{ijkl} are the photoelastic tensor components, n is the refractive index of the material and S_{kl} the components of the strain tensor, ω and Ω are the optical and acoustic frequencies, respectively, and M_{eff} is the effective motional mass related to the normalized acoustic displacement field by $M_{\mathrm{eff}} = \rho\int_V \|\mathbf{U}\|^2\,\mathrm{d}V$, where ρ is the mass density. The total OM coupling rate g is then given by $g = g_{\mathrm{PE}} + g_{\mathrm{MI}}$.

In addition to the above method, we have also developed a simulation method [20–23,28] in which the strength of the OM interaction is obtained from the modulation of the cavity photon frequency by the cavity phonon, namely the frequency of the photonic mode is calculated at successive instants of an acoustic period under the assumption that the acoustic mode strain profile is being frozen at these instants. This hypothesis is justified by the fact that the frequency of the phonon is several orders of magnitude below the photon frequency. In these simulations, it is necessary to give a magnitude to the acoustic strain inside the cavity. For the sake of numerical computations, we assume in general a maximum strain in the cavity equal to 1%. However, this is actually much higher than more realistic values of 10^{-4} to 10^{-6} that can be expected from an external acoustic source exciting the phononic cavity mode. Let us briefly discuss this point. When the amplitude of the acoustic wave is very small, the simulation method becomes equivalent to the first-order perturbation theory where only first-order phonon processes can occur. In this case, the optical modulation behaves like a sine function during one period of the acoustic vibration (as we shall see in the illustrations given in the next sections), and the amplitude of this modulation is proportional to the amplitude of the acoustic strain. However, when the acoustic wave becomes stronger, higher order phonon processes become also possible, although in practice the first-order term may remain often predominant. Then, the optical modulation can deviate from a sinusoidal behavior and the strengths of the higher-order processes can be deduced from the Fourier components of the optical modulation during one period of the acoustic wave [23]. Therefore, the simulation method becomes also useful to discuss non-linear effects involving several phonons in the acousto-optic interaction phenomena. Additionally, the first-order contribution to the coupling rate may vanish in some cases due to symmetry reason and only higher-order phonon exchanges become allowed. For instance, we have observed in such cases [23] that the optical modulation behaves like the square of a sine function, with its amplitude being proportional to the square of the strain. This shows that two-phonon processes occur and are now predominant.

Considering different cavities in phoxonic crystals, we have applied the above methodology to each pair of localized phonon and photon. In particular, we have discriminated the pairs that give a zero coupling to the first order for symmetry reasons. The above methods allow us to compare the relative contributions of the PE and MI mechanisms and in particular their relative sign, which defines whether the two contributions add to, or partly cancel, each other. Finally, the contributions of the PE mechanism are compared in crystal structures based on Si and GaAs to elucidate the material and wavelength dependence [45] of the photoelastic parameters.

3. Cavity optomechanics

In this section we give a few selected illustrations of the photon–phonon interaction in different cavities in 2D, slab and nanobeam structures. First, we consider a 2D phoxonic crystal made of a square lattice of holes in Si with lattice parameter a and the radius of the holes equal to $r/a = 0.48$ and introduce a L_1 cavity by removing one hole. This cavity supports 6 localized phononic modes and 3 TE and 5 TM optical modes appearing in their respective gaps. These modes can be classified according to their symmetry, even (E) or odd (O) with respect to two symmetry planes of the cavity. From a survey of Eqs. (1)–(2), one can demonstrate [23] that a non-degenerate photonic mode can only couple a phononic mode of EE symmetry, independently of its own symmetry. However, for a degenerate photonic mode, a coupling with phonons of other symmetry becomes possible. In Fig. 1, we give the coupling rates as well as the modulations of all TM photonic modes of the cavity with one of the phononic mode representing a breathing deformation of the cavity. Indeed, the latter gives the highest coupling strength [22,23], in particular because the PE and MI effects add to each other. Let us notice that this

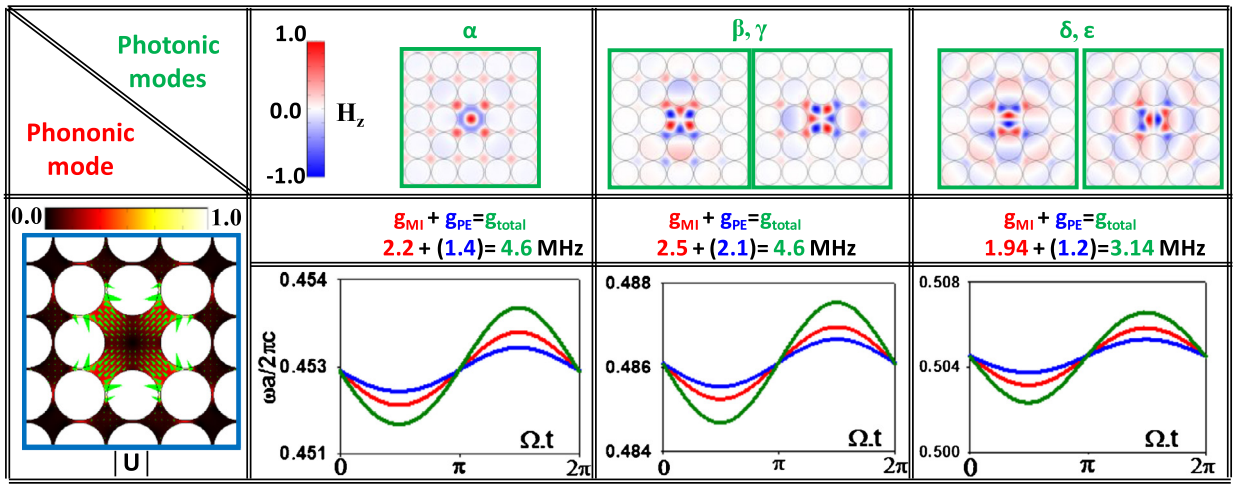

Fig. 1. Optomechanic interaction in the L_1 cavity of a 2D phoxonic crystal. The figure presents the modulation of the TM modes α, (β, γ), and (δ, ε) during one period $T = 2\pi/\Omega$ of the acoustic vibrations associated with a breathing phononic mode. The moving interface (MI, red lines), the photo-elastic (PE, blue lines) and the full acousto-optic coupling (MI + PE, green lines) are represented for each photonic mode.

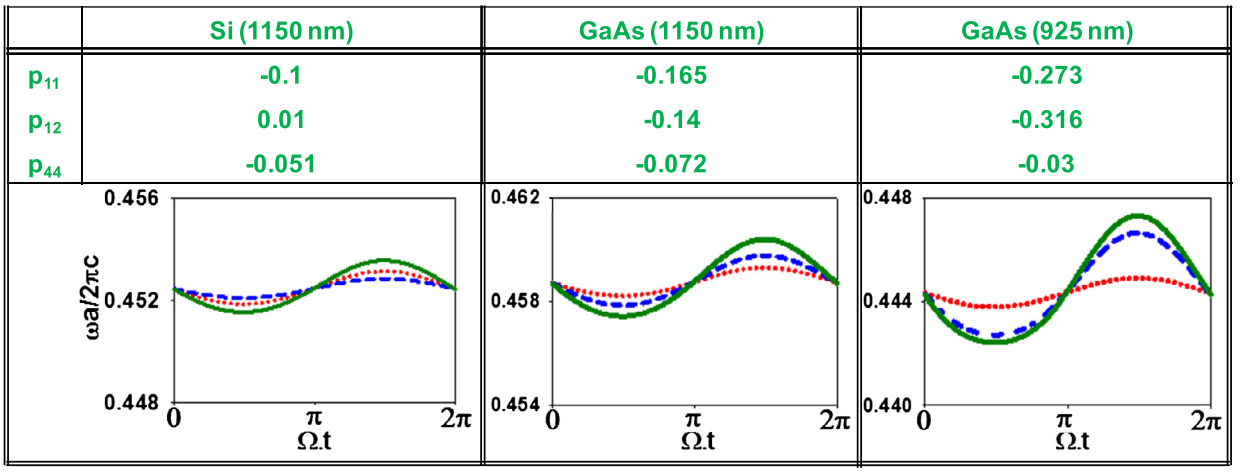

Fig. 2. Modulation of the optical mode α by the same acoustic mode as in Fig. 1. The plots compare the moving interface (MI, red lines), photo-elastic (PE, blue lines) and full acousto-optic (MI + PE, green lines) couplings between three cases: (a) Si, (b) GaAs at $\lambda_1 = 1150$ nm and (c) GaAs at $\lambda_2 = 925$ nm. In each case, the photoelastic parameters which are material and wavelength dependent are given in the upper panel.

vibrational motion does not leave the degeneracy of the photonic modes (β, γ), and (δ, ε) and all the modulations show a sinusoidal behavior during one period of the acoustic vibration. Additionally, one can notice a proportionality between the modulation amplitudes and the magnitudes of the coupling rate g. The coupling with other phonons give different behaviors, in particular the PE and MI effects can partly cancel each other, the degeneracy of the photonic modes can be lifted, or the coupling rate can vanish to the first order of perturbation theory. The details are given in Ref. [23].

To show the sensitivity of the PE effect to the choice of the material and the wavelength [45], we present in Fig. 2 the modulation of the optical mode α by the same acoustic mode as before in two phoxonic crystals made respectively of Si and GaAs. Additionally, the results in GaAs are given at two wavelengths, one relatively far from the electronic band gap of the semiconductor and the other close to this band gap, where the photoelastic parameters can display large variations. The strength of the PE coupling appears higher in GaAs than in Si, especially when the wavelength approaches the band gap and the PE effect becomes much more dominant with respect to the MI effect.

The 2D crystal is interesting for the purpose of basic physical discussions. But in actual structures, the photonic modes can leak from the cavity and have only a limited quality factor which is an important factor for the experimental observation of the optical frequency shift due to the acoustic mode. As an illustration, we consider the case of the same L_1 cavity, but now in a square lattice of holes in a silicon slab [46]. The thickness of the slab and the radius of the holes are respectively $0.6a$ and $0.43a$, where a is the lattice parameter, fixed to 540 nm. This phoxonic crystal displays (see Fig. 3) a narrow phononic absolute gap in the range of 5.86–6.19 GHz, contained in a much broader phononic gap (from 5 to 6.76 GHz) for the modes which have an even symmetry with respect to the middle plane of the slab. It also shows a photonic gap

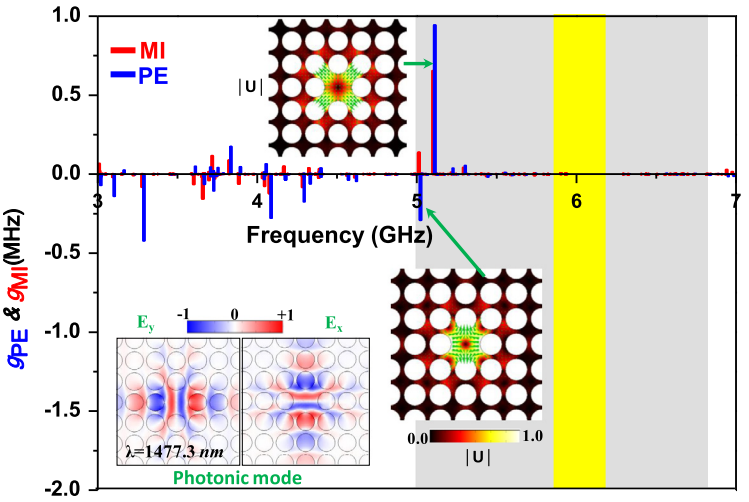

Fig. 3. Optomechanic interaction in the L_1 cavity of a phoxonic crystal slab. The figure presents the coupling rates g_{MI} (in red) and g_{PE} (in blue) of the photonic mode at $\lambda = 1477.3$ nm with all the phononic modes in the structure. Significant PE and MI coupling rates are obtained with two acoustic modes at 5.1 and 5 GHz that are inside the phononic gap of even symmetry (grey area). However, only the former gives a high total coupling rate because the PE and MI contributions add to each other. The maps of the fields are also presented.

of even symmetry at [1455–1608 nm]. The L_1 cavity supports a localized photonic mode in the gap at 1477.3 nm which however displays a poor quality factor Q of about 1000. Fig. 3 shows the coupling rate of this mode with all the acoustic modes (extended and localized) in the crystal structure. It is worthwhile noticing that due to symmetry reasons, the optical mode can only couple with phononic modes that have an even symmetry with respect to the middle plane of the slab. The highest coupling rate is obtained for a phononic mode at 5.1 GHz located in the gap of even symmetry (and not in the absolute gap) for which the PE and MI contributions add to each other. Another mode at 5.0 GHz displays a non-negligible, although much lower, coupling rate because of the partial cancellation between PE and MI contributions. We have also studied other cavities such as L_3 and cross-shape cavities [28]. Although strong coupling rates can be obtained, which are similar or higher than in the literature, the drawback of these cavities remains the low values of the quality factors for their photonic modes which can become a limitation to the experimental observation of optomechanical effects. One can expect that these quality factors can be improved by making a design of the holes surrounding the cavity.

In the last part of this section, we briefly present the results of our calculations for an original 1D phoxonic nanobeam structure [20,21,46] that can support cavity photonic modes of high quality factors and displaying high phonon–photon coupling rates. Some of the theoretical predictions have already been demonstrated experimentally [21,47]. The strip consists of a backbone containing a periodic array of holes at the middle and a periodic array of stubs on each side (Fig. 4(a)), the former and the latter being respectively favorable to the opening of the photonic and phononic band gaps (Figs. 4(b) and (c)).

The geometrical parameters are $r = 0.3a$, $e = 0.44a$, $L = a$, and $d = 0.5a$, where a is the lattice parameter fixed at 500 nm. The dispersion curves are classified with colors according to their symmetry (even or odd) with respect to the two symmetry planes Π' and Π of the nanobeam. The photonic band structure displays a gap of OE symmetry and the acoustic band structure contains two absolute as well as a few symmetry-dependent gaps. It is worthwhile noticing that, to the first order of perturbation theory, the OM coupling does not vanish only for phonons that have the EE symmetry. For this reason, the localized phonons in a cavity can be preferentially searched in the gaps associated with the EE modes, as represented in Fig. 4(c). Additionally, if the cavity has itself a symmetry plane at its middle (which is often the case), the only active phononic modes will be those with EEE symmetry.

In a recent work [46], we studied several types of cavities in the above nanobeam. Here we show a few illustrations for a cavity in which both the OM coupling rate and the quality factors of the photonic modes are found to be sufficiently high. To fulfill the latter condition, it is necessary to design a tapered cavity such as in Fig. 5, where the geometrical parameters present a gradual variation from the center of the cavity towards both ends, where they reach their values in the perfect crystal. In the structure of Fig. 5(a), the period and hole size are progressively reduced towards the cavity center to 70% of their bulk values with a parabolic shape, whereas the height of the stubs are kept constant.

This cavity supports several photonic modes in the range of 1500–1600 nm achieving high quality factors of about $2 \cdot 10^5$. The calculation of the coupling rates with all the acoustic modes of the structure reveals that those falling in the range of absolute band gaps around 3.7 GHz give relatively low coupling rates (below 0.6 MHz) with all the cavity photonic modes. Instead, two resonant modes with frequencies outside the band gaps, respectively at 2.46 and 6.35 GHz, give the strongest coupling.

The first mode, shown in Fig. 5(a), corresponds to a breathing motion of several stubs at the center of the cavity vibrating all in phase. This mode originates from the flat EE dispersion curve in the vicinity of the Γ point of the Brillouin zone in this frequency range.

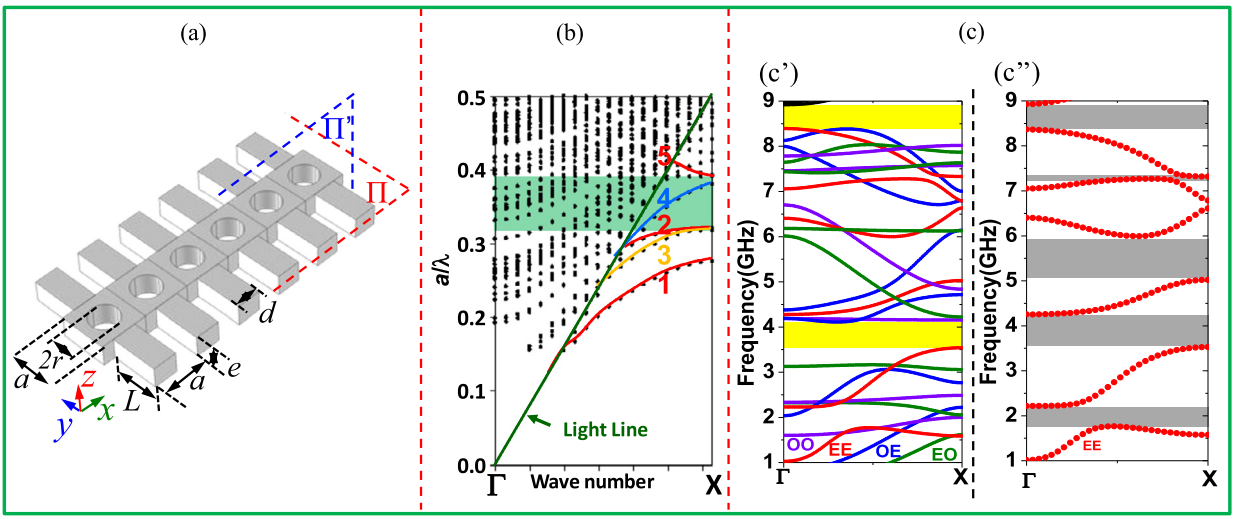

Fig. 4. (a) Schematic representation of the corrugated nanobeam containing holes in the middle and stubs grafted on each side. Π and Π' are the symmetry planes of the nanobeam. (b) Photonic band structure showing the existence of a gap with OE symmetry (green area). (c) Phononic band structure where the bands of different symmetries with respect to the planes Π' and Π are shown with different colors. (d) Same as (c), but keeping only the dispersion curves with EE symmetry (in red). The EE symmetry gaps are presented in grey and the absolute band gaps in yellow.

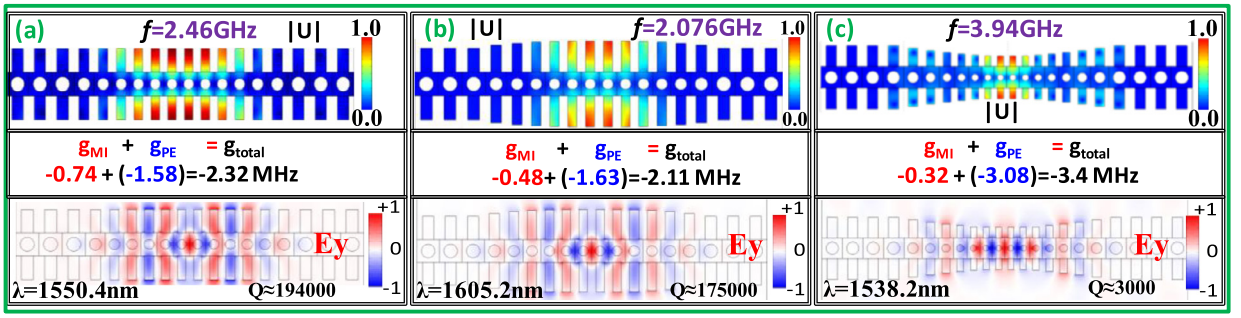

Fig. 5. Tapered cavity while the height of the stubs is: (a) kept constant; (b) increases towards the cavity center; (c) decreases towards the cavity center. The figure presents the maps of the fields as well as the coupling rates g_{PE}, g_{MI} and g_{total}.

It shows high coupling rates with all the optical cavity modes among them one example is presented in Fig. 5(a). The second acoustic mode at 6.35 GHz corresponds also to a higher-order breathing motion of the stubs, together with a significant localization in the backbone of the nanobeam. It couples strongly with one of the photonic mode with a coupling rate of 2.47 MHz. However, this mode is more sensitive to the details of the geometrical parameters than the former, which remains robust with respect to such variations.

Despite the high photonic quality factor and the strong OM coupling, the drawback of the previous structure is that the involved phononic modes are located outside the gaps and thus can radiate out of the cavity. To overcome this inconvenience, we propose pushing the mode at 2.46 GHz either downwards into the nearby EE symmetry gap, or upwards into the absolute band gap. These operations become possible by changing (respectively increasing or decreasing) gradually the height of the stubs from the periphery towards the cavity center. The results are respectively presented in Figs. 5(b) and (c).

The gradual increase in the length of the stubs (Fig. 5(b)) brings the acoustic mode at 2.07 GHz, inside the EE symmetry gap. The quality factors of several photonic modes are conserved as well as the high coupling rates. The drawback of this situation is that the acoustic mode may still leak out of the cavity if the cavity does not fully satisfy the symmetry properties due to some imperfections in the fabrication of the nanobeam structure. From this point of view, the situation where the height of the stubs is gradually decreased (Fig. 5(c)) allows us to push the acoustic mode to the absolute gap, thus preventing more efficiently the leakage. The inconvenience in this case is that the original acoustic mode needs to be shifted by a large amount (from 2.46 to 3.94 GHz), so the tapering of the cavity becomes less efficient to keep very high quality factors of the photonic modes. This drawback may be improved by using less abrupt tapering in this case.

Based on the above theoretical predictions, several corrugated nanobeams with various tapering were fabricated and their OM properties investigated. Some results are detailed in [21,47]. In particular, it is observed that the phononic modes around 2.5 GHz with strong OM coupling are almost common to all samples, while higher phononic modes up to 7 GHz are more sensitive to the details of the geometrical structure such as the shift in the exact positions of the holes or deviation

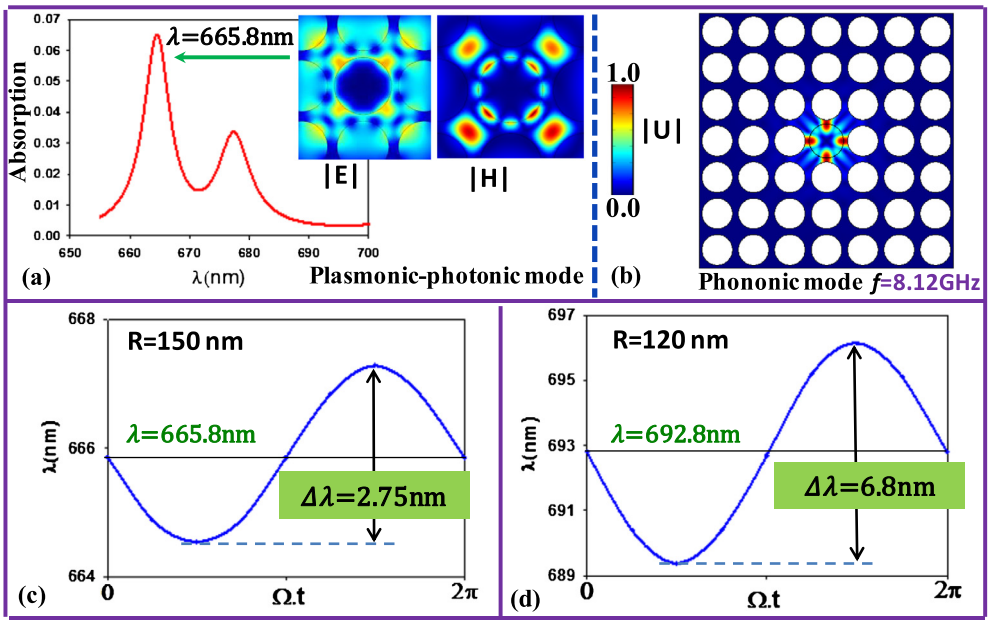

Fig. 6. Optomechanic interaction in a L_1 cavity containing a gold nanowire in a 2D TiO_2 photonic crystal. (a) Absorption spectrum for a wire of radius 150 nm located at the cavity center and map of the electromagnetic field for the coupled photon–plasmon modes of the cavity. (b) Map of a phononic mode in the cavity. (c) Modulation of the absorption peak by the acoustic mode. (d) Same as (c) for a wire of radius 120 nm.

from their circular shape, or the rounding of the stubs at their basis. Therefore, it becomes necessary to simulate the exact shape of the nanobeam as obtained from SEM images to explain the effect of the microfabrication imperfections on the very high frequency acoustic modes. Interestingly, some of the unwanted imperfections happen in a systematic way rather than randomly, so the experimental observations of the OM effects can found general explanations.

4. Cavity optomechanics in presence of a metallic nanoparticle

Localized surface plasmons (LSP) on metallic nanoparticles have been extensively studied [48,49] for their fundamental properties and applications in several fields such as biosensing [50,51], surface enhanced Raman spectroscopy, photothermal therapy [52], metamaterial behaviors.... For some applications as in biosensing, the resonances need to be as narrow as possible to detect a small change in their frequencies. In a very recent paper [53], we studied the behavior of LSP when a gold nanowire is introduced in a cavity inside a 2D photonic crystal. In particular, it was shown that "a wire with diameter about the lattice constant presents very narrow resonances corresponding to hybrid photonic–plasmonic modes, where increased lifetime is attributed to the decrease of the radiative losses by interaction with the photonic crystal." It is worthwhile noticing that the plasmonic resonances are often characterized by their absorption rather than their transmission spectrum.

In this section, we present some preliminary extensions of this work to the evaluation of the OM interaction in a photonic cavity containing a metallic nanowire. For the sake of simplicity, we use the same model as in [53], namely cylindrical gold nanowires in a L_1 cavity in a 2D photonic crystal made of a square array of holes in a TiO_2 matrix. The choice of the matrix is dictated by the fact that TiO_2 is transparent in the range of visible light where the Au plasmonic properties are investigated. Also, here we limit ourselves to a 2D crystal while dealing with more realistic situations of a cavity in a slab or nanobeam would be feasible with more computational effort. It should be pointed out that the dielectric constant of Au is complex and frequency dependent in the visible optical range and the data for the finite element simulations are taken from Ref. [54].

The geometrical parameters of the photonic crystal are $a = 320$ nm and $r/a = 0.42$ for the hole radius. This crystal has an absolute gap in which two localized modes can be found [53]. Due to their symmetry, both of them have a vanishing electric field at the cavity center. This means that if the Au nanowire is placed at the center of the cavity, its effect can become significant only if its radius is not too small. For this reason, in the following, we consider two situations, one in which the nanowire is placed at the cavity center and its radius is around 150 nm, and another situation where the wire is displaced from the center along the diagonal of the cavity.

Fig. 6 gives an example of the first situation where the Au nanowire is located at the center of the cavity. The absorption spectrum (Fig. 6(a)) displays two peaks which are much narrower than if the wire were in a homogeneous TiO_2 background, although they are much broader than usual transmission peaks in photonic crystals. They are reminiscent of photon–plasmon coupling inside the cavity [53]. Then, we calculate the strength of the OM interaction due to the MI mech-

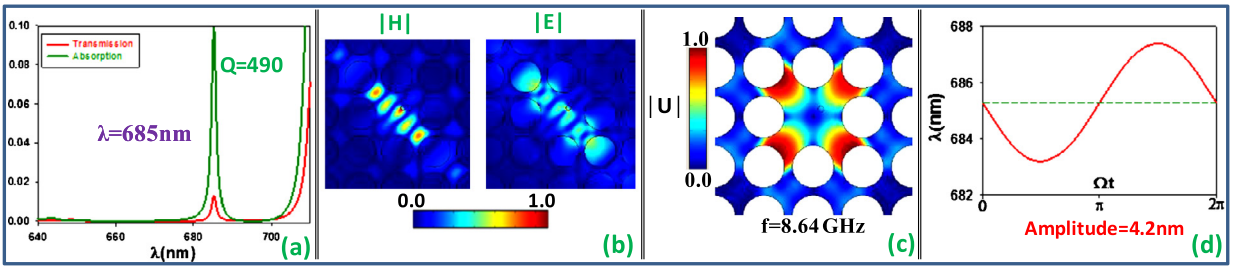

Fig. 7. Same as in Fig. 6 for a small gold nanowire of radius 20 nm displaced from the center of the cavity towards the corner by 70.7 nm.

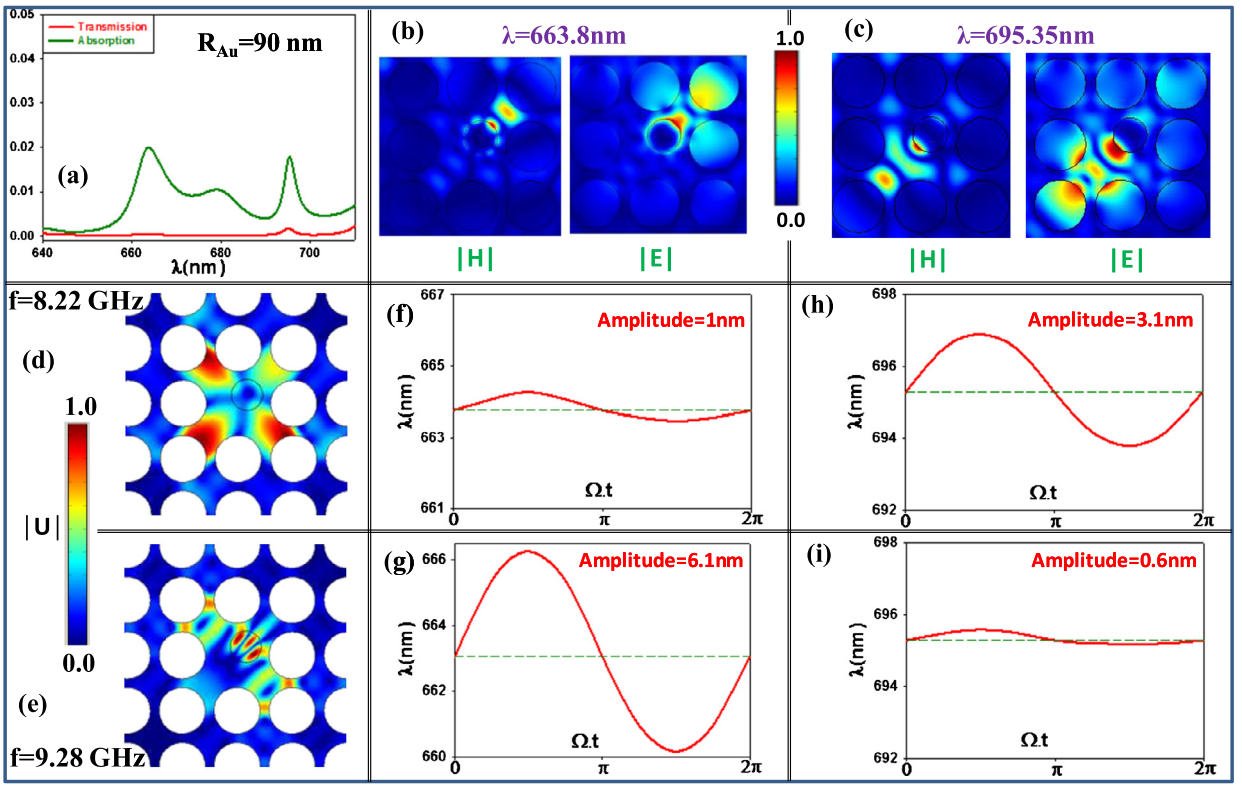

Fig. 8. Same as in Figs. 6 and 7 for a gold nanowire of radius 90 nm displaced from the center of the cavity towards the corner by 70.7 nm. The figures show the modulations of two plasmon–photon modes by two phononic modes of the cavity.

anism with the only phononic mode of the cavity (Fig. 6(b)) that gives a significant coupling. The latter mainly corresponds to a stretching motion along the diagonals of the cavity with significant deformations both at the Au–TiO_2 and TiO_2-holes boundaries. The magnitude of the absorption peak modulation (Fig. 6(c)) is of the same order of magnitude as those found in Section 3 for cavity OM. This modulation amplitude increases when the wire radius decreases from 150 to 120 nm, while the wavelength of the absorption peak increases from 665 to 692 nm.

Now, we assume that the Au nanowire is displaced along a diagonal of the cavity by an amount of 70.7 nm (i.e. 50 nm along each of the x and y directions) in order that its position coincide with the maximum of the electric field for one of the cavity photonic mode. Then, its radius is progressively increased from 10 to 100 nm. A small wire such as in Fig. 7 changes only slightly the photonic and phononic modes of the original cavity. For instance, the degeneracy of the photonic mode is lifted and one of the two modes remains inside the band gap (Figs. 7(a) and (b)). The change in the phononic mode shown in Fig. 7(c) is even weaker due to the fact that the main localization of this mode happens towards the corners of the cavity. We show in Fig. 7(d) the modulation of the absorption peak by the acoustic vibration, and a relatively strong coupling is obtained.

By increasing the size of the nanowire, its effect on the existence and field distribution of the localized modes become progressively more noticeable. We illustrate in Fig. 8 the case of a gold nanowire of radius 90 nm. Now, the absorption spectrum contains much broader resonances than previously, which are characteristic of plasmon–photon coupling modes (Fig. 8(a)) and their fields show an enhancement at the metal surface (Figs. 8(b) and c). We show also two phononic

modes of the cavity (Figs. 8(d) and (e)) where the mode at 8.22 GHz remains only slightly deformed with respect to the one obtained with a small nanowire (Fig. 7(c)), whereas the mode at 9.28 GHz is mainly localized in one side of the Au nanowire and the surrounding space. The calculation of the OM interaction between each pair of the photonic and phononic modes reveals that the phonon at 8.22 GHz modulates more strongly the photonic mode at 695 nm than the one at 663 nm, because their overlap is stronger, as can be seen from the maps of the fields. The opposite situation occurs for the phonon at 9.28 GHz, which has a high overlap with the photonic mode at 663 nm, but almost none with the mode at 695 nm.

These preliminary investigations of the OM interaction in a photonic cavity containing a metal nanowire show several possibilities for obtaining strong modulation of the absorption spectrum of coupled photon–plasmon modes.

5. Conclusion

We have presented a brief review of our recent calculations of cavity OM interaction in several phoxonic crystals including 2D, slab and nanobeam structures. By taking into account both PE and MI mechanisms of acousto-optic interaction, we have evaluated the strength of the OM coupling either by a first-order perturbation theory or by a simulation method that gives the modulation of an optical cavity mode by an acoustic mode. The results of the two methods are consistent and allow us to compare the strength of the OM coupling for each phonon–photon pair, as well as to compare the relative contributions of the PE and MI effects. It is worthwhile noticing that these two mechanisms can act constructively or destructively depending on the relative signs of their contributions. Also, from symmetry consideration, one can discriminate the pairs of phonon–photon for which first-order perturbation theory yields a vanishing coupling rate. Then, the simulation method allows evaluating the importance of non-linear processes that involve the exchange of more than one phonon. Based on the theoretical predictions, several corrugated nanobeam structures have been fabricated and showed strong coupling rates of a few MHz with high-quality-factor photonic modes and acoustic modes up to a few GHz. Finally, we presented some new results about the extension of the preceding works to the case where a gold nanowire is inserted into the photonic cavity. By varying the size of the wire in the range of 10–150 nm and its position from the cavity center towards the cavity corner, we have shown that strong OM coupling with coupled plasmon–photon modes is also possible.

References

[1] Y. Pennec, J. Vasseur, B. Djafari-Rouhani, L. Dobrzynski, P.A. Deymier, Surf. Sci. Rep. 65 (2010) 229.
[2] M.I. Hussein, M.J. Leamy, M. Ruzzene, Appl. Mech. Rev. 66 (2014) 040802.
[3] M. Maldovan, Nature 503 (2013) 209.
[4] W. Aspelmeyer, T.J. Kippenberg, F. Marquardt, Rev. Mod. Phys. 86 (2014) 1391.
[5] Markus Aspelmeyer, Pierre Meystre, Keith Schwab, Phys. Today 65 (2012) 29.
[6] M.S. Kushwaha, P. Halevi, L. Dobrzynski, B. Djafari-Rouhani, Phys. Rev. Lett. 71 (1993) 2022.
[7] M.M. Sigalas, E.N. Economou, Solid State Commun. 86 (1993) 141.
[8] E. Yablonovitch, Phys. Rev. Lett. 58 (1987) 2059.
[9] J.D. Joannopoulos, R.D. Meade, J.N. Winn, Molding the Flow of Light, Princeton University Press, Princeton, NJ, USA, 1995.
[10] M. Trigo, A. Bruchhausen, A. Fainstein, B. Jusserand, V. Thierry-Mieg, Phys. Rev. Lett. 89 (2002) 227402;
N.D. Lanzillotti-Kimura, A. Lemaitre, A. Fainstein, B. Jusserand, B. Perrin, Phys. Rev. B 84 (2011) 115453;
A. Fainstein, N.D. Lanzillotti-Kimura, B. Jusserand, B. Perrin, Phys. Rev. Lett. 110 (2013) 037403.
[11] I.E. Psarobas, N. Papanikolaou, N. Stefanou, B. Djafari-Rouhani, B. Bonello, V. Laude, Phys. Rev. B 82 (2010) 174303.
[12] E. Almpanis, N. Papanikolaou, N. Stefanou, Opt. Express 22 (2014) 31595.
[13] M. Maldovan, E.L. Thomas, Appl. Phys. B 83 (2006) 595;
M. Maldovan, E.L. Thomas, Appl. Phys. Lett. 88 (2006) 251907.
[14] D. Bria, M.B. Assouar, M. Oudich, Y. Pennec, J. Vasseur, B. Djafari-Rouhani, J. Appl. Phys. 109 (2011) 014507.
[15] S. Sadat-Saleh, S. Benchabane, F.I. Baida, M.P. Bernal, V. Laude, J. Appl. Phys. 106 (2009) 074912.
[16] Y. Pennec, B. Djafari-Rouhani, E.H. El Boudouti, C. Li, Y. El Hassouani, J.O. Vasseur, N. Papanikolaou, S. Benchabane, V. Laude, A. Martinez, Opt. Express 18 (2010) 14301.
[17] S. Mohammadi, A.A. Eftekhar, A. Khelif, A. Adibi, Opt. Express 18 (2010) 9164.
[18] Y. El Hassouani, C. Li, Y. Pennec, E.H. El Boudouti, H. Larabi, A. Akjouj, O. Boumatar, N. Papanikolaou, S. Benchabane, V. Laude, A. Martinez, B. Djafari-Rouhani, Phys. Rev. B 82 (2010) 155405.
[19] Y. Pennec, B. Djafari-Rouhani, C. Li, J.M. Escalante, A. Martinez, S. Benchabane, V. Laude, N. Papanikolaou, AIP Adv. 1 (2011) 041901.
[20] M. Oudich, S. El-Jallal, Y. Pennec, B. Djafari-Rouhani, J. Gomis-Bresco, D. Navarro-Urrios, C.M. Sotomayor Torres, A. Martıınez, A. Makhoute, Phys. Rev. B 89 (2014) 245122.
[21] J. Gomis-Bresco, D. Navarro-Urrios, M. Oudich, S. El-Jallal, A. Griol, D. Puerto, E. Chavez, Y. Pennec, B. Djafari-Rouhani, F. Alzina, A. Martínez, C.M. Sotomayor Torres, Nat. Commun. 5 (2014) 4452.
[22] Q. Rolland, M. Oudich, S. El-Jallal, S. Dupont, Y. Pennec, J. Gazalet, J.C. Kastelik, G. Lévêque, B. Djafari-Rouhani, Appl. Phys. Lett. 101 (2012) 061109.
[23] S. El-Jallal, M. Oudich, Y. Pennec, B. Djafari-Rouhani, A. Makhoute, Q. Rolland, S. Dupont, J. Gazalet, J. Phys. Condens. Matter 26 (2014) 015005.
[24] T.-X. Ma, K. Zou, Y.-S. Wang, C. Zhang, S. Xiao-Xing, Opt. Express 22 (2014) 28443.
[25] E. Gavartin, R. Braive, I. Sagnes, O. Arcizet, A. Beveratos, T.J. Kippenberg, Phys. Rev. Lett. 106 (2011) 203902.
[26] D.A. Fuhrmann, S.M. Thon, H. Kim, D. Bouwmeester, P.M. Petroff, A. Wixforth, H.J. Krenner, Nat. Photonics 5 (2011) 605.
[27] A.H. Safavi-Naeini, O. Painter, Opt. Express 18 (2010) 14926.
[28] S. El-Jallal, M. Oudich, Y. Pennec, B. Djafari-Rouhani, V. Laude, J.-C. Beugnot, A. Martıınez, J.-M. Escalante, A. Makhoute, Phys. Rev. B 88 (2013) 205410.
[29] A.H. Safavi-Naeini, J.T. Hill, S. Meenehan, Jasper Chan, Simon Gröblacher, Oskar Painter, Phys. Rev. Lett. 112 (2014) 153603.
[30] T.-R. Lin, Y.-C. Huang, J.-C. Hsu, J. Appl. Phys. 117 (2015) 173105.
[31] M. Eichenfield, J. Chan, R.M. Camacho, K.J. Vahala, O. Painter, Nature 462 (2009) 78.
[32] M. Eichenfield, J. Chan, A.H. Safavi-Naeini, K.J. Vahala, O. Painter, Opt. Express 17 (2009) 20078.
[33] J. Chan, A.H. Safavi-Naeini, J.T. Hill, S. Meenehan, O. Painter, Appl. Phys. Lett. 101 (2012) 081115.

[34] P.T. Rakich, C. Reinke, R. Camacho, P. Davids, Z. Wang, Phys. Rev. X 2 (2012) 011008.
[35] F.-L. Hsiao, C.-Y. Hsieh, H.-Y. Hsieh, C.-C. Chiu, Appl. Phys. Lett. 100 (2012) 171103.
[36] J.-Charles Beugnot, V. Laude, Phys. Rev. B 86 (2012) 224304.
[37] J.-C. Beugnot, S. Lebrun, G. Pauliat, H. Maillotte, V. Laude, T. Sylvestre, Nat. Commun. 5 (2014) 5242.
[38] T.-R. Lin, C.-H. Lin, J.-C. Hsu, J. Appl. Phys. 113 (2013) 053508.
[39] Y. Pennec, V. Laude, N. Papanikolaou, B. Djafari-Rouhani, M. Oudich, S. El-Jallal, J.-C. Beugnot, J.M. Escalante, A. Martínez, Modeling light-sound interaction in nanoscale cavities and waveguides, Nanophotonics (2014), http://dx.doi.org/10.1515/nanoph-2014-0004.
[40] T.J. Kippenberg, K.J. Vahala, Science 32 (2008) 1172.
[41] I. Favero, K. Karrai, Nat. Photonics 3 (2009) 201.
[42] D. Royer, E. Dieulesaint, Elastic Waves in Solids II: Generation, Acousto-Optic Interaction, Applications, Springer, 1999.
[43] B. Djafari-Rouhani, E.M. Khourdifi, Localized and extended acoustic waves in superlattices. Light scattering by longitudinal phonons, in: D.L. Lockwood, J.F. Young (Eds.), Light Scattering in Semiconductor Structures and Superlattices, in: NATO ASI Ser., Ser. B: Phys., vol. 273, Plenum Press, 1991, pp. 139–158.
[44] S.G. Johnson, M. Ibanescu, M.A. Skorobogatiy, O. Weisberg, J.D. Joannopoulos, Y. Fink, Phys. Rev. E 65 (2002) 066611.
[45] P. Renosi, J. Sapriel, Appl. Phys. Lett. 64 (1994) 2794.
[46] B. Djafari-Rouhani, S. El-Jallal, M. Oudich, Y. Pennec, AIP Adv. 4 (2014) 124602.
[47] D. Navarro-Urrios, J. Gomis-Bresco, S. El-Jallal, M. Oudich, A. Pitani, N. Capuj, A. Tredicucci, A. Griol, Y. Pennec, B. Djafari-Rouhani, A. Martinez, C.M. Sotomayor Torres, AIP Adv. 4 (2014) 124601.
[48] S.A. Maier, Plasmonics: Fundamentals and Applications, Springer US, Boston, MA, USA, 2007.
[49] A. Akjouj, G. Levêque, S. Szunerits, Y. Pennec, B. Djafari-Rouhani, R. Boukherroub, L. Dobrzynski, Nanometal plasmon polaritons, Surf. Sci. Rep. 68 (2013) 1–67.
[50] J.J. Mock, D.R. Smith, S. Schultz, Nano Lett. 3 (2003) 485.
[51] O. Saison-Francioso, G. Lévêque, A. Akjouj, Y. Pennec, B. Djafari-Rouhani, S. Szunerits, R. Boukherroub, J. Phys. Chem. C 116 (2012) 17819.
[52] D. Jaque, L. Martiınez Maestro, B. Del Rosal, P. Haro-Gonzalez, A. Benayas, J.L. Plaza, E. Martin Rodriguez, J. Garcia Sole, Nanoscale 6 (2014) 9494.
[53] A. Mrabti, S. El-Jallal, G. Lévêque, A. Akjouj, Y. Pennec, B. Djafari-Rouhani, Combined photonic–plasmonic modes inside photonic crystal cavities, Plasmonics (2015), http://dx.doi.org/10.1007/s11468-015-9932-3.
[54] P.B. Johnson, R.W. Christy, Phys. Rev. B 6 (1972) 4370.